Viscous drag effect in the flexural rigidity and cantilever stiffness of bio- and nano-filaments measured with the shooting-bead method

Abdorreza Samarbakhsh* and Jack. A. Tuszynski†
Department of Physics, University of Alberta, 11322-89 Avenue, Edmonton, Alberta, Canada T6G 2G7
(Received 28 November 2008; revised manuscript received 25 May 2009; published 2 July 2009)

The so-called shooting-bead method is a fast and easy experimental technique for evaluating cantilever stiffness and flexural rigidity of semiflexible to semirigid rodlike biological and nano-filaments based on the measurement of just two distances. In this paper we have derived the shooting-bead formula for cantilever stiffness and flexural rigidity taking into account the effects of the viscous drag force exerted on the filament itself. To this end, we have defined a key variable, called the filament energy-loss factor (or filament drag factor), which accounts for all the energy-loss effects. It has been shown that due to the logarithmic dependence of the filament energy-loss factor on the radius and the length of the filament, inclusion of this factor in the formula for the flexural rigidity has a very noticeable effect on the result even for very thin or long filaments. It has also been shown that the effect due to the consideration of filament energy-loss factor on calculation of the flexural rigidity increases with increasing the flexibility of the filament. We have also considered various sources of experimental error and estimated their effects.

DOI: 10.1103/PhysRevE.80.011903 PACS number(s): 87.80.Ek, 87.80.Cc

I. INTRODUCTION

When viewing the individual living cell as a nanomechanical and nanoelectronic device, we need to know what the physical properties of its internal hardware are. Interiors of living cells are structurally organized by the cytoskeleton networks of filamentous polymers whose biomechanical properties are of key interest to biophysicists. With few exceptions, the filaments of importance to the cell are all made up of protein polymers.

The cytoskeletal network of filaments has the responsibility of defining cell shape, protecting the cell from changes in osmotic pressure, organizing its contents, providing cellular motility, and finally is responsible for separating chromosomes during mitosis. Protein filaments of the cytoskeleton consist of actin [micro-filaments (MFs)], intermediate filaments (IFs), and microtubules (MTs). Throughout the cell a network of contractile actin bundles exerts tension and pulls the cell's membrane toward the nucleus at the core. MTs resist the compressive force of the actin cables providing a balance. IFs provide additional structural stability.

Micro-filaments are single-stranded filaments, with diameters of approximately 3–6 nm and variable lengths. Microfilaments are found linked together by actin-associated proteins and congregate into one of the three major forms. There are over 100 different actin-binding proteins responsible for actin associating with the membrane, with membrane-bound receptors and with ion channels, as well as for promoting assembly and causing the depolymerization of those filaments. Actin-binding proteins, such as ARP2/3 and profilin, regulate micro-filament assembly. Actin depolymerizing factor/cofilin stimulates disassembly. Gelsolin caps fast-growing ends of filaments and may also be involved in filament disassembly.

Microtubules are long hollow filaments consisting of bound α-tubulin and β-tubulin monomers. MT polymerization can be controlled by temperature and pH—a concentration of protein and ions to produce closely or widely spaced MTs, centers, sheets, rings, and even the so-called macrotubes that have diameters in the range of 200–500 nm and are polymerized with the influence of an elevated zinc ion concentration [1]. Assembled microtubules have outer diameters of 25–26 nm and inner diameters of 15 nm and typically contain 13 protofilaments when assembled *in vivo*. MTs are made up of 12–17 protofilaments under *in vitro* conditions. Each protofilament is shifted lengthwise with respect to its neighbor describing left-handed helical pathways around the MT. Like actin filaments, microtubules have plus and minus ends. Polymerization or elongation occurs preferentially at plus ends and depolymerization or shortening occurs at minus ends. Microtubule associated proteins (MAPs) are tissue and cell-type specific and represent several classes with different functions. General classes are minus-end binding, plus-end binding (e.g., the kinetochore of mitotic chromosomes, polymer severing, polymer stabilizing) and cross-linking (i.e., MAP-2 and tau in neurons), and motor proteins. These microtubule binding proteins determine the architecture of microtubules and microtubule assemblies.

All of the above cellular protein filament structures have significant persistence lengths that increase with the molecular mass of the building block and related mechanical stability and rigidity that are of growing interest to physicists. F-actin can support large stresses [2] without a great deal of deformation and it ruptures at approximately 3.5 $\mathrm{N/m^2}$. Ma *et al.* [3] showed that IFs resist high applied pressures by increasing their stiffness. They can withstand higher stresses than the other two components without sustaining mechanical damage [2]. By biological standards, MTs are rigid polymers with a large persistence length [4] of 6 mm. From experiments of Janmey *et al.* [2], MTs exhibit a larger strain for

*Author to whom correspondence should be addressed; asamar@phys.ualberta.ca
†Also at Division of Experimental Oncology, Cross Cancer Institute, 11560 University Avenue, Edmonton, AB, Canada T6G 1Z2.

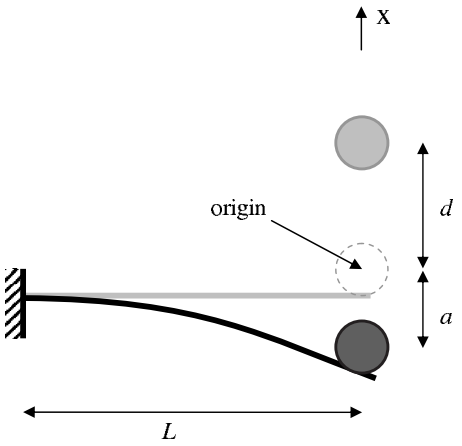

FIG. 1. Schematic illustration of the two states of the rodlike biological filament and the bead. First, the filament has been pushed by a bead inside an optical trap and second, when the filament has been released and the bead has come to rest asymptotically. (Figure not to scale, usually a, d, and R are much smaller than L).

a small stress compared [3] to either MFs or IFs. The rupture stress for MTs is very small and typically is only about $0.4-0.5$ N/m^2. The lateral contacts between tubulin dimers in neighboring protofilaments play a decisive role in MT stability, rigidity, and architecture [5]. Tubulin dimers are relatively strongly bound in the longitudinal direction (along protofilaments), while the lateral interaction between protofilaments is much weaker [6]. There have been a number of theoretical [7,8] and experimental [9] studies in recent years dealing with the various aspects of the elasticity of MTs.

In this paper we propose a simple method of determining the stiffness of semiflexible polymers such as MTs or indeed bundles of such filaments [10] and provide a theoretical framework for interpreting the experimental results. One of the main issues in this paper is not only the analysis of the shooting-bead method [11] as applied to the nano- and biofilaments but, more specifically, how the drag forces exerted on the filament present in the viscous medium affect the energy loss and consequently the measurement's results. This method is especially suited for stiff filaments or their bundles (e.g., cilia, flagella, macrotubes, or MAP–interconnected MT bundles in axons). Even for individual microtubules, where Taute *et al.* [12] determined that filament drag is a major effect for the bending of MTs, the length of the filament makes a crucial difference to the cantilever stiffness such that short MTs become stiffer and the resultant motion of the bead is underdamped making the method applicable. Moreover, the method described below can be readily utilized for nanotechnologically produced filaments such as single-walled or multiwalled carbon nanotubes (CNTs) [13] that provide an excellent system for calibration and control.

II. CONCEPTUAL BASIS

In Fig. 1 we show a schematic of two states of a typical semiflexible rodlike bio- or nano-filament, which is clamped at one end to a pivot point and whose other (free) end first has been pushed down by a bead inside an optical trap [14,15] and then has been released by turning the laser trap off. The cantilever stiffness of a rod with length L is k and the radius of the bead is denoted as R. Typical bead diameters are approximately $1-2$ μm (with focused laser, it is possible to trap beads with a radius as low as 200 nm), while the rod diameters range between 100 nm for microtubule bundles, 200–500 nm for macrotubes, and about 500 nm for cilia. Also nanotechnology methods allow us to make filaments from different materials with controlled values of their radii. For example, it is now possible to make single-walled or multiwalled CNTs with different radii ranging from a few to 100 nm.

In this paper, our primary aim is to expand the proposed method for measuring filament stiffness in order to include the effects of the energy loss due to the viscous drag force exerted on the filament itself and to make the final shooting-bead formula as accurate as possible. While the commonly employed wormlike chain model has become standard in the description of semiflexible and flexible polymers such as DNA, this is not a necessary level of approximation for stiffer filaments that have long persistence lengths such as MTs, cilia, flagella, or CNTs where small deflection approximation can be warranted. For example, the mm-range persistence lengths and a high level of rigidity characteristic of MTs translate into a picture where a significant thermal fluctuation in shape occurs over tens to hundreds of thousands of constituent dimers. In this paper we also wish to provide a means of estimating experimental errors for the shooting-bead formula and assess under which instrumental resolution this method will be able to work. To make the paper self-contained and use the results of the intermediate steps yielding the first shooting-bead formula [11] (when the bead's diameter is much larger than that of the rod), in this section we briefly explain the concepts involved in the method.

Assuming that we can keep the rod in its bent conformation over a certain period of time, we can now imagine that if we suddenly turn the optical trap (laser tweezer) off, the force holding the rod down is abruptly removed. Hence, the bead that was pushing down on the free end of the rod while in the trap will now experience a reaction force from the tip of the rod leading to its displacement from its previous position. The amount of displacement a when moving the bead downward in the initial phase of the experiment will determine the initial position of the bead at the time of releasing it from the tip of the rod. Following the release of the bead from the laser trap, the bead will jump up. The motion of the bead can be analyzed in terms of two contributions. First, the bead experiences two forces, an upward force due to the cantilever stiffness of the rod and a downward viscous drag force (there are two other forces; Appendix A provides an additional explanation of the effects created by these forces). The equation of motion for the bead together with the initial conditions is given below:

$$m\dot{x} = -kx - 6\pi\eta R\dot{x}, \quad x(0) = -a, \quad \dot{x}(0) = 0. \tag{1}$$

Note that m and η represent the mass of the bead and viscosity of the solution, respectively. The solution of Eq. (1)

with the initial conditions, which corresponds to underdamped motion, is [16]

$$x(t) = -a\exp\left(-\frac{3\pi\eta R}{m}t\right)\cos\left[\sqrt{\frac{k}{m}-\left(\frac{3\pi\eta R}{m}\right)^2}\,t\right]. \quad (2)$$

The motion will be underdamped if the bead passes through the origin and this condition applies to a rigid rod and/or low viscous solution.[1] In the second part of the motion ($x \geq 0$), the bead experiences just a downward viscous drag force. This motion starts from the moment when the bead passes through the origin at a time instant equal to $t_0 = \pi/2\sqrt{\frac{k}{m}-(\frac{3\pi\eta R}{m})^2}$ in the first part of the motion. As a result, the equation for the bead's position as a function of time is [11]

$$x(t) = \frac{ma}{6\pi\eta R}\sqrt{\frac{k}{m}-\left(\frac{3\pi\eta R}{m}\right)^2}\exp\left[-\frac{3\pi^2\eta R}{2m\sqrt{\frac{k}{m}-\left(\frac{3\pi\eta R}{m}\right)^2}}\right] \times\left[1-\exp\left(-\frac{6\pi\eta R}{m}t\right)\right]. \quad (3)$$

Note that in the above equation we have shifted our initial time from $t=t_0$ to $t=0$. Since $x(t\to\infty)=d$ [due to the exponential dependence of $x(t)$ on t just after passing a few intervals of $\tau=m/6\pi\eta R$, *asymptotic approach time constant*, we can consider the bead as being at rest] solving Eq. (3) for k and using the Euler-Bernoulli bending formula [17] for small deflection, we can find the following formula (which will be referred to as the first shooting-bead formula) for flexural rigidity[2] of the filament:

$$\kappa = \frac{1}{3}kL^3 = \frac{9\pi\eta^2 L^3}{4\rho R}\left(\frac{\pi^2}{4\left[W\left(\frac{\pi a}{4d}\right)\right]^2}+1\right). \quad (4)$$

Note that the symbol W in the above equation is called the *Lambert W* function[3] [18]. Since it is easier to determine the density of the bead, ρ, compared to its mass, we have changed our variable from mass of the bead to its density at this final point. This will also help in reducing the error when calculating the error propagation for our formula if the original information is based on the knowledge of the density and radius of the bead.

To simplify the notation, we define the following new variables for future calculations:

[1]Theoretically it is always possible to have an underdamped motion for the bead by making the value of the quantity under the square root in Eq. (2) positive. Even if we do not have an underdamped motion for the bead at the beginning, by cutting the filament to a shorter length we can make k large enough (as we know, k is inversely proportional to the third power of the length of the filament) to end up with a positive value for the quantity under the square root.

[2]As flexural rigidity (or bending stiffness) is the product of the Young modulus, E, of the filament material and the second moment of area, I, of the filament cross section, it is very common to use EI instead of κ for flexural rigidity.

[3]It is also called the omega function or product logarithmic function.

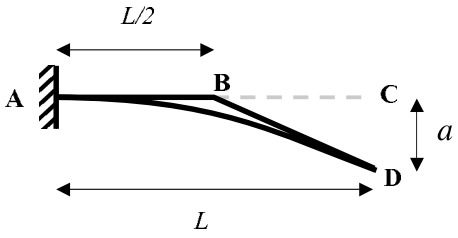

FIG. 2. Representation of the filament as a rotating rigid rod with the length of $L/2$. (Deflection angle CBD is exaggeratedly shown).

$$\Lambda = \frac{3\pi\eta R}{m}, \quad \Omega = \sqrt{\frac{k}{m}-\left(\frac{3\pi\eta R}{m}\right)^2}. \quad (5)$$

III. ENERGY CONSERVATION AND FILAMENT ENERGY-LOSS CONSIDERATION

In Sec. II the problem at hand has been solved analytically by including the net force exerted on the bead but ignoring the force exerted on the filament by the solution. It is a good idea to investigate our solution from the conservation of energy point of view at this stage. Since this part can be considered as a totally separate part and in order to maintain the main flow of the paper, this part has been moved to the appendix. The interested reader can see the proof in Appendix B.

Looking at the problem from the energy point of view will guide us to define a very important parameter that can help us to provide an estimate of the energy loss due to the viscous force exerted on the filament based on the bead's energy loss.

In this section we intend to estimate the energy loss of the filament (Q_{1R}) and compare it with the energy loss of the bead (Q_{1B}) and the total energy loss (Q_{1T}) during the first part of the motion. To solve the problem analytically we approximate the motion of the bent filament as a rotating rod with the length of $L/2$ (see Fig. 2). This is a good approximation because for a small deflection, the area swept by the rod compared to the area swept by the whole filament amounts to more than 2/3 (see Appendix C for a mathematical proof of this statement).

The viscous drag torque exerted on the rod (BD) with radius r that rotates with angular velocity ω inside a medium with viscosity η is equal to [9]

$$T = \frac{\frac{1}{6}\pi\eta L^3}{\ln\left(\frac{L}{2r}\right)-0.66}\omega. \quad (6)$$

The infinitesimal energy loss of the rod when it rotates by $d\theta$ is therefore

$$dQ_{1R} = \frac{\frac{1}{6}\pi\eta L^3}{\ln\left(\frac{L}{2r}\right)-0.66}\omega d\theta = \frac{\frac{1}{6}\pi\eta L^3}{\ln\left(\frac{L}{2r}\right)-0.66}\omega^2 dt. \quad (7)$$

Here dt denotes the elapsed time for such an infinitesimal rotation.

As we know, the tip of the filament pushes on the bead, which means that the velocity of the tip is the same as the

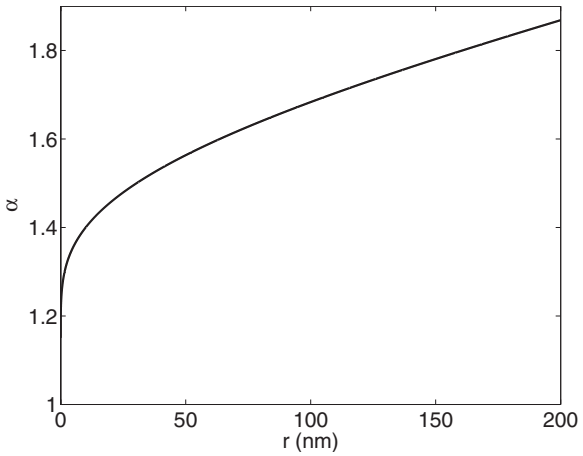

FIG. 3. Filament energy-loss factor as a function of filament radius for a 10 μm filament and a 1 μm bead diameter.

velocity of the bead at any time during the first part of the motion. Thus using $v=L\omega/2$ we find

$$dQ_{1R}=\frac{\frac{2}{3}\pi\eta L}{\ln\left(\frac{L}{2r}\right)-0.66}v^2dt. \tag{8}$$

To calculate the energy loss of the rod we have to integrate an expression based on Eq. (8) but at this stage we cannot do this yet because the equation of motion for the bead (the system composed of the bead and the filament) does not remain the same as before (when we ignored that filament energy loss). For this reason we just find the ratio of the filament energy loss to the bead energy loss at the moment as this ratio plays an important role in our calculation. Namely,

$$\frac{Q_{1R}}{Q_{1B}}=\frac{\int dQ_{1R}}{\int dQ_{1B}}=\frac{1}{9\frac{R}{L}\left[\ln\left(\frac{L}{2r}\right)-0.66\right]}=\alpha-1. \tag{9}$$

Therefore, knowing the radius of the filament, the length of the filament and the radius of the bead α can be found. Note also that α is the ratio of the total energy loss to the bead energy loss that has a value greater than 1 and we refer to it as the *filament energy-loss factor* or *filament drag factor*.

Figure 3 shows the filament energy-loss factor as a function of the filament radius for a 10-μm-long filament and 1 μm bead diameter. It should be stressed that although we have found the ratio of Q_{1R}/Q_{1B}, we are not able to calculate the filament energy loss at this stage. The reason for this is that Q_{1B} does not remain the same as before in the case when filament energy loss is ignored [see Eq. (B4) or (B7) in Appendix B). This means that the following relation is *not* correct:

$$Q_{1R}=(\alpha-1)Q_1=\frac{1}{2}(\alpha-1)ma^2\Lambda^2 \times\left(\frac{\pi^2}{4\left[W\left(\frac{\pi a}{4d}\right)\right]^2}\left\{1-\exp\left[-2W\left(\frac{\pi a}{4d}\right)\right]\right\}+1\right). \tag{10}$$

To calculate the correct filament energy loss we first need to evaluate the new equation of motion (that will be solved in Sec. IV) and then we need to follow all the steps that we took to reach Eq. (B4) or (B7) for finding a new solution.

IV. EFFECTS OF FILAMENT ENERGY LOSS ON DIMENSIONLESS FLEXURAL RIGIDITY CURVE

In this section we derive two equations for calculating the cantilever stiffness and flexural rigidity with consideration of filament energy loss. The equation of motion for the system (bead+filament) is

$$(I_B+I_R)\ddot{\theta}=-k\left(\frac{L}{2}\right)^2\theta-\frac{\frac{1}{6}\pi\eta L^3}{\ln\left(\frac{L}{2r}\right)-0.66}\dot{\theta}-6\pi\eta\left(\frac{L}{2}\right)^2\dot{\theta}. \tag{11}$$

Here, θ is the angle between the rod and the undeflected filament (the angle between BD and BC in Fig. 2). Assuming that r, a, and R are all much smaller than L and using the definition of the filament energy-loss factor, the above equation becomes

$$\frac{I_B+I_R}{\left(\frac{L}{2}\right)^2}\ddot{\theta}=-k\theta-6\pi\eta\alpha R\dot{\theta}. \tag{12}$$

Using the moment of inertia for a single particle (keeping in mind that the radius of the bead is much smaller than the length of the filament) with mass m and moment of inertia for a rigid rod with length $L/2$ and mass m_R, as well as the relation between x and $\theta(x=L\theta/2)$, we obtain

$$\left(m+\frac{1}{3}m_R\right)\ddot{x}=-kx-6\pi\eta\alpha R\dot{x}. \tag{13}$$

Generally 1/6 of the mass of the filament is much smaller than the mass of the bead. For example, even for a solid filament (many bio-filaments or bundles of them can be considered to have hollow interiors such as microtubules or macrotubes) with a radius of 100 nm (that would be a very thick filament) and with a 10 μm length and the density of water, the effect of ignoring the mass of the filament with respect to the mass of the bead with a radius of 1 μm and the same density is just 3.75%. Now, comparing the above equation with Eq. (1) and eliminating m_R, we notice that the only difference between these equations amounts to the replacement of η with $\alpha\eta$. It means that we can use the solution of that equation (with the same initial conditions) as a solution of Eq. (13) where η is rescaled to become $\alpha\eta$.

Defining the following new variables,

$$\Lambda'=\frac{3\pi\alpha\eta R}{m},\quad \Omega'=\sqrt{\frac{k}{m}-\left(\frac{3\pi\alpha\eta R}{m}\right)^2}, \tag{14}$$

we find

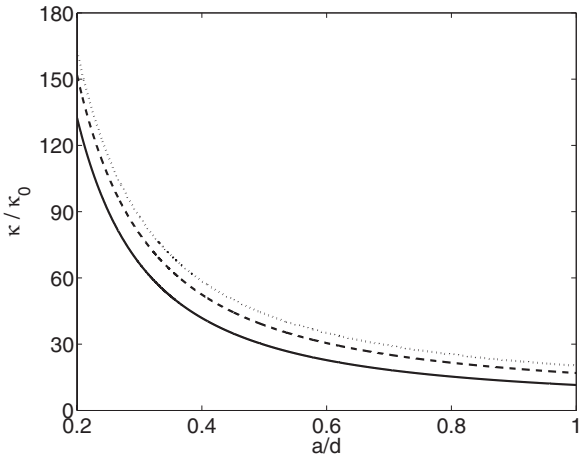

FIG. 4. A plot of the dimensionless flexural rigidity κ/κ_0 as a function of a/d for a 10 μm filament and 1 μm bead diameter for three different situations: (a) the solid curve, without filament energy-loss consideration (which corresponds to the filament energy-loss factor of 1.0), (b) the dashed curve for a 50 nm filament radius that corresponds to a filament energy-loss factor of 1.562, and (c) the dotted curve for a 200 nm filament radius that corresponds to a filament energy-loss factor of 1.868.

$$x(t) = -a\,\exp(\Lambda' t)\cos(\Omega' t). \tag{15}$$

It is clear that the second part of the motion of the bead when it passes through the origin will satisfy the same differential equation of motion but this time the initial condition for the velocity will change to

$$\dot{x}(0) = a\Omega'\,\exp\left(-\frac{\pi\Lambda'}{2\Omega'}\right). \tag{16}$$

As a result, the equation for the bead's position as a function of time changes to

$$x(t) = \frac{a\Omega'}{2\Lambda}\exp\left(-\frac{\pi\Lambda'}{2\Omega'}\right)[1-\exp(-2\Lambda t)]. \tag{17}$$

Since $x(t\to\infty)=d$ and using some algebra we arrive at

$$s'\,\exp(s') = \frac{\pi\alpha a}{4d}, \tag{18}$$

where s' is a dimensionless variable equal to $\frac{\pi\Lambda'}{2\Omega'}$.

The cantilever stiffness and the flexural rigidity will be found from the following equations:

$$\kappa = \frac{1}{3}kL^3 = \frac{9\pi\eta^2 L^3}{4\rho R}\left(\frac{\pi^2\alpha^2}{4\left[W\left(\frac{\pi\alpha a}{4d}\right)\right]^2}+\alpha^2\right). \tag{19}$$

Again we have changed our variable from mass of the bead to its density in the last step. Note that the above formula for the cantilever stiffness and flexural rigidity (the second shooting-bead formula) for the case of $\alpha=1$ reduces to the first shooting-bead formula (when the filament energy loss is not taken into account).

Figure 4 shows the effects of filament energy-loss consideration on the dimensionless flexural rigidity [11] curve as a function of a/d for three different filament radii, which corresponds to three different values of the filament energy-loss factor. To calculate the cantilever stiffness and the flexural rigidity for any other radius, first the filament energy-loss factor is calculated from Eq. (9) and then this value is substituted into Eq. (19). As is clear from the graph for a single value of the ratio of a/d, the dimensionless flexural rigidity increases as a function of the filament energy-loss factor. This is easy to understand since a higher fraction of the bending potential energy of the filament will be used to cancel out the energy loss of the filament due to viscous drag torque.

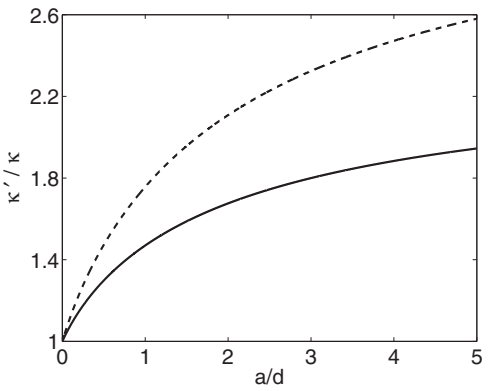

FIG. 5. A plot of a ratio of the flexural rigidity with consideration of the filament energy-loss factor, κ', to flexural rigidity without consideration of the filament energy-loss factor, κ, as a function of a/d for two filaments considered in Fig. 4: (a) the solid curve for a 50 nm filament radius that corresponds to a filament energy-loss factor of 1.562 and (b) the dashed curve for a 200 nm filament radius that corresponds to a filament energy-loss factor of 1.868.

Another important outcome that we can conclude from the effect due to the filament energy-loss factor on the dimensionless flexural rigidity curve is dependency of this effect on the ratio of a/d. Figure 5 shows the ratio of the flexural rigidity with consideration given to the filament energy-loss factor, κ', to the flexural rigidity without considering the filament energy-loss factor, κ, as a function of a/d for the two previously considered filaments.

As we see from this graph, κ'/κ increases for any filament (with the inclusion of the filament energy-loss factor) when a/d increases. We also see from Fig. 4 that when a/d increases for a filament with a known radius and length and also a known bead's radius (this means that we know the filament energy-loss factor), the dimensionless flexural rigidity decreases. This leads us to state the following important result: *consideration of the filament energy loss (or filament drag) is more important for filaments with less rigidity than for stiff ones*.

Since our answer is parametric and flexural rigidity depends on the values of a/d, L, r, R, η, and ρ we can end up with a wide range of values for flexural rigidity (note that the method works provided the bead passes through the origin, which means when we have underdamped motion for the bead), but we give a rough estimate of the flexural rigidity value based on our pilot experiment (not reported in this paper due to its preliminary character). For an approximately 10 μm filament length, 100 nm filament radius (made from

tubulin dimers; see Sec. VI), 1 μm bead radius, immersed in an aqueous solution, and also with $a=d=1$ μm, we end up with 10^{-17} for the order of magnitude in SI units of the flexural rigidity estimate. We expect that with different values for length and a/d the result may decrease by a few orders of magnitude. Therefore, our method is concluded to be most suitable for rigid filaments such as MT bundles, cilia, and especially single-walled and multiwalled CNTs [13].

Stiff filament approximation

For stiff filaments we have a condition $\alpha a/d \ll 1$ and hence we can keep just the first term of the expansion of $s' \exp(s')$ in Eq. (18). In that case, the filament's cantilever stiffness and flexural rigidity can be found from the following formula:

$$\kappa = \frac{1}{3}kL^3 = \frac{9\pi\eta^2 L^3}{\rho R}\left(\frac{d^2}{a^2}\right). \tag{20}$$

In the last step to reach Eq. (20) we ignored $\alpha^2/4$ with respect to d^2/a^2 that directly follows from our approximation. Note that in the case of the stiff filament approximation there is no dependence on the filament energy-loss factor because in that case the area swept by the filament is very small (due to a small value of a with respect to d). This is also clear from Fig. 5 when both curves approach unity at $a/d=0$ regardless of the amount of filament energy-loss factor.

V. SOURCES OF ERROR

In this section we wish to analyze the role of various sources of experimental error in the evaluation of the filament stiffness. To reach that goal, first we derive an equation for the percentage error for the first shooting-bead formula based on the error in our measurable quantities a and d (also η, ρ, L, and R when calculating $\delta\kappa_0$). In the second part of this section we consider the effects of thermal diffusion and will demonstrate that using modern instruments these effects are expected to be relatively small.

A. Error calculation for the first shooting-bead formula

Since it is our intention to derive an error formula for the most general case we perform error calculations for the dimensionless flexural rigidity. At the end, knowing the error of κ_0, we can calculate the final error for the flexural rigidity (see Appendix D for the calculation of $\delta\kappa_0$ and $\delta\kappa$). Taking the differential of Eq. (4) gives

$$\delta\left(\frac{\kappa}{\kappa_0}\right) = \frac{\kappa}{\kappa_0}\frac{2\pi^2\delta W}{4W^3+\pi^2 W}, \tag{21}$$

but we know from Eq. (18) that

$$\delta W = \left(\frac{\delta a}{a}+\frac{\delta d}{d}\right)\frac{W}{1+W}. \tag{22}$$

Note also that as we are calculating the error for the first shooting-bead formula we should consider $\alpha=1$ in order to get the above equation.

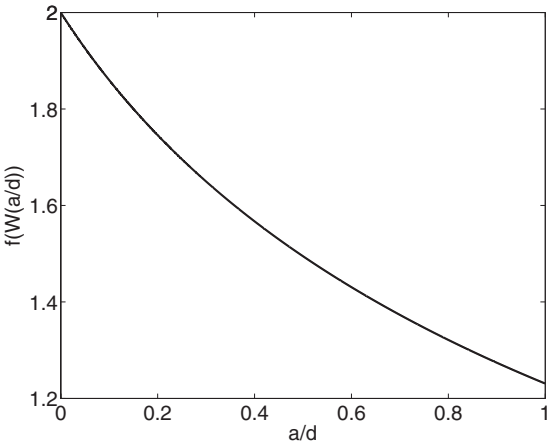

FIG. 6. Plot of the last ratio in Eq. (23), $f(W)=2\pi^2/[(1+W)(\pi^2+4W^2)]$, as a function of a/d.

Substituting Eq. (22) into Eq. (21) we obtain

$$\delta\left(\frac{\kappa}{\kappa_0}\right) = \frac{\kappa}{\kappa_0}\left(\frac{\delta a}{a}+\frac{\delta d}{d}\right)\frac{2\pi^2}{(1+W)(\pi^2+4W^2)}. \tag{23}$$

To calculate the percentage error in the measurement of dimensionless flexural rigidity, first we have to evaluate the last ratio in Eq. (23). Figure 6 shows this ratio in Eq. (23) as a function of a/d. Measuring a/d, we need to find the corresponding value for this ratio from this graph but to facilitate the use of the above formula, we notice that the last denominator in Eq. (23) is a monotonically increasing function on the entire domain of W that has its global minimum equal to π^2 at the beginning of the domain of W (at $W=0$ that corresponds to $a/d=0$). This means we can estimate an upper limit for the error calculation for the dimensionless flexural rigidity as

$$\delta\left(\frac{\kappa}{\kappa_0}\right) \leq \frac{\kappa}{\kappa_0}2\left(\frac{\delta a}{a}+\frac{\delta d}{d}\right). \tag{24}$$

Measuring a and d and knowing the resolution of the instrument, we can estimate the upper limit for the percentage error for the dimensionless flexural rigidity from the above formula. To provide a rough estimate of the error in this method, we consider $a=d=1$ μm (these are very close values to those seen in our preliminary experiment). With an accurate instrument it is possible to measure distances as small as 0.1 nm. Reference [19] provides some information about high-resolution single-molecule measurements. Here, we consider $\delta a=\delta d=1$ nm to obtain a conservative estimate for the percentage error. Substituting the above values to Eq. (24) we obtain 0.4% for the upper limit [the actual value found using Eq. (23) or Fig. 6 is 0.25%] of the percentage error for the dimensionless flexural rigidity.

B. Diffusion

For large beads, more than a 1 μm in radius, random thermal motion is not very pronounced (it has not been observed in our preliminary experiment) but we nevertheless wish to calculate the effects of thermal diffusion in a general case for this experiment in this section.

We know that the diffusion constant for a spherical bead with radius R at temperature T is $k_BT/6\pi\eta R$. Also the relation between the mean square displacement, $(\Delta X)^2$, and time, t, involves the diffusion constant D as a proportionality constant [20], i.e., $(\Delta X)^2=2Dt$. Combining the two equations we obtain

$$(\Delta X)^2 = \frac{k_BT}{3\pi\eta R}t. \tag{25}$$

The elapsed time for the damped motion of the bead is on the order of asymptotic approach time constant τ. For example, after a period of 9τ, the bead passes 99.988% of its final displacement (the number 9 has been used to simplify the answer), thus using the definition of τ and the above equation, the root mean square of the displacement due to the diffusion can be found as

$$\Delta X = \left(\frac{2k_BT\rho R}{3\pi\eta^2}\right)^{1/2}. \tag{26}$$

At $T=25$ °C, in an aqueous solution for a bead with 1 μm radius and a density equal to that of water we find $\Delta X=0.935$ nm. This is a relatively small value that can serve as an approximate measure of the experimental error in the bead position for our calculation.

VI. DISCUSSION AND CONCLUSION

In our preliminary experiment [21] some tubulin-based biotinylated bio-filaments have been produced due to the spontaneous aggregation of the tubulin dimers in the laboratory sample. Estimating the dimensions of the filaments observed in the solution (approximately 20–30 μm in length and 200 nm in width), we surmise that these semiflexible objects were composed of microtubule bundles consisting of several or more microtubules in a bundle. While the diameter of a microtubule is 25 nm, the spatial resolution of the images was not sufficient to ascertain how far apart each microtubule was in a bundle. Since the images indicate splaying apart of bio-filaments at far ends of some of the bundles, we conclude that these were not individual macrotubes but several microtubules forming a bundle. During the experiment (when pushing the tip of a clamped bio-filament by a streptavidin coated bead to create an attachment point), we observed a strange effect involving a catapultlike release of the microbead from the filament and a subsequent projectile motion until it stopped following a very rapid movement through the solution. Seeing this effect that can be described as a "jumping bead" phenomenon in the laboratory was the main motivation behind our effort to find a physical description reported in the present paper. While the experiment itself is still in progress, the method proposed here allows us to probe one of the important characteristics of stiff bio-filaments and nano-filaments with a very fast and relatively uncomplicated measurement of the initial and final positions of the bead. Also, knowing precisely the cross section of the filament and measuring the associated flexural rigidity, we are able to calculate the Young modulus of the filament.

In conclusion, we note that the method presented in this paper offers numerous advantages over the other methods currently in use (e.g., the buckling force method [22,23], the hydrodynamic flow method [24,25], the wiggle and relaxation methods [26,27], or the thermal fluctuation technique [28]) for the reasons listed below:

For this experiment, the bead needs not be attached to the filament; actually, this was one of the reasons that guided the introduction of the proposed method. It needs just a single trap, there is no need to find the force exerted on the bead by the trap, there is no need to know the exact shape of the filament, there is no need to oscillate the trap, there is no need to measure the time, and there is no need to measure the velocity of the bead or the rod. The only measurement that we need to perform is the measurement of the length for a and d; also because the ratio of a/d is important and not a and d individually, there is no need to calibrate the microscope.

Another aspect that we should briefly discuss here is the logarithmic dependence of the viscous drag torque exerted on the filament on the radius and length of the filament. Even for a thin filament it is important to consider the effects of filament energy-loss factor on the dimensionless flexural rigidity curve. Figure 3 shows that even for small values of the filament radius, the filament energy-loss factor is not very close to 1. This is also clear from Fig. 4, as we see the dimensionless flexural rigidity curve for the filament with a 50 nm radius (the dashed curve) is much closer to the dimensionless flexural rigidity curve for the filament with a 200 nm radius (the dotted curve) compared with the curve without filament energy-loss consideration (the solid curve).

Also dependence of the dimensionless flexural rigidity on the length of the filament via the filament energy-loss factor is very important. Even for a small radius of the filament compared to the bead's radius if we increase L, L varies much faster than $\ln(L)$ in Eq. (9). Therefore, α will have a considerable value.

Ultimately we demonstrated that the effect due to the filament energy-loss factor on the dimensionless flexural rigidity curve increases as a/d increases. As we know, when this ratio increases for a filament with a known radius and length and also a known radius of the bead, the (dimensionless) flexural rigidity decreases. This means consideration of the filament energy loss (or filament drag) is more important for filaments with less rigidity.

ACKNOWLEDGMENTS

A.S. wishes to thank Dr. Linda Payet for performing the preliminary experiment and providing the images. Help and assistance of Neda Naseri and Michelle Hanlon in providing the graphs and illustrations is greatly appreciated. A.S. also acknowledges support from the University of Alberta. This research was supported by grants from NSERC of Canada, the Alberta Cancer Foundation, and the Allard Foundation awarded to J.A.T.

APPENDIX A: CALCULATING THE ORDER OF MAGNITUDES FOR VERTICAL DISPLACEMENT DUE TO THE BUOYANT FORCE AND THE WEIGHT OF THE BEAD

It has been assumed that the density of the bead is equal or close to the density of the solution (in most cases this will

be composed mainly of water), which means that the buoyant force and the weight of the bead cancel each other out. Therefore, we need not make a correction for the apparent weight of the bead, but this method still works even if the density of the bead is different from the density of the solution because of the following two reasons. Referring to Fig. 1, which is in a horizontal plane, the vertical forces (the effects of gravity and buoyant forces) do not provide any contribution to the horizontal motion. Second, the experiment pertains to a process that occurs in a fraction of a second that depends on an asymptotic approach time constant. In this appendix we estimate how much the bead moves vertically during the experiment assuming the density of the bead is different from the density of the solution. If this distance, b, is large with respect to the length of the focal region of the microscope, the resolution of the image of the bead after the experiment will be lost.

The vertical force exerted on the bead is $|m-m_s|g$, where m_s denotes the displaced mass of the solution. Therefore, the vertical acceleration of the bead is

$$a_z = \frac{m-m_s}{m}g. \tag{A1}$$

The elapsed time for this motion is on the order of the asymptotic approach time constant; therefore the total vertical distance is on the order of $g(m-m_s)(9\tau)^2/2m$ or

$$b \sim O\left(\frac{9}{8}mg\frac{|m-m_s|}{\pi^2\eta^2R^2}\right). \tag{A2}$$

With a typical value of $\eta=10^{-3}$ Pa·s for water and $R=1$ μm, $m_s=\frac{1}{2}m\simeq 4\times 10^{-15}$ kg for aqueous solution, we obtain $b\sim O(10^{-13})m$.

This means that the vertical displacement due to the buoyant force and the weight of the bead during the experiment is definitely negligible and we will not lose the focus when viewing the bead after it stops.

APPENDIX B: ENERGY CONSERVATION INVESTIGATION

It is important to validate the solution by making sure that the initial potential energy of the filament is equal to the total energy loss (Q) of the bead due to the viscous drag force exerted on it over the course of its motion. Infinitesimal energy loss of the bead during its motion is given by

$$dQ = -dW_v = -F_v dx = 6\pi\eta R\dot{x}^2 dt. \tag{B1}$$

Note that in the above equation we calculate the negative of the work done on the bead by the viscous drag force in order to arrive at a positive value for the energy loss of the system. The value of $\dot{x}^2$ can be found by taking the derivative of Eq. (2) and squaring it, so that

$$\dot{x}^2 = a^2\exp(-2\Lambda t)(\Lambda^2\cos^2\Omega t + \Omega^2\sin^2\Omega t + \Lambda\Omega\sin 2\Omega t). \tag{B2}$$

From Eqs. (B1) and (B2) we obtain

$$Q_1 = 3\pi\eta R a^2\int_0^{t_0}\exp(-2\Lambda t)[\Lambda^2+\Omega^2+(\Lambda^2-\Omega^2)\cos 2\Omega t + 2\Lambda\Omega\sin 2\Omega t]dt. \tag{B3}$$

The subscript 1 in Q_1 indicates that this is energy loss that occurred in the first part of the motion (underdamped harmonic motion from $t=0$ to $t=t_0=\pi/2\Omega$). The result of the above equation is

$$Q_1 = \frac{1}{2}ka^2 - \frac{1}{2}ma^2\Omega^2\exp\left(-\frac{\Lambda}{\Omega}\pi\right). \tag{B4}$$

Energy loss in the second part of the motion (damped motion) can be found using the following integral:

$$Q_2 = 6\pi\eta R\int_0^{\infty}a^2\Omega^2\exp\left(-\frac{\Lambda}{\Omega}\pi\right)\exp(-4\Lambda t)dt = \frac{1}{2}\frac{3\pi\eta R}{\Lambda}a^2\Omega^2\exp\left(-\frac{\Lambda}{\Omega}\pi\right). \tag{B5}$$

From Eqs. (B4) and (B5) we find that the total energy loss of the bead during its whole motion is exactly equal to the potential energy stored in the filament just before releasing the bead. This then validates the solutions we found earlier in the paper.

Although to prove the conservation of energy we did not need to calculate the bead energy loss in terms of measurable quantities a and d; for completeness of the solution we evaluate Q_1 in terms of those quantities. In order to do that we have to replace k and Ω in Eq. (B4) in terms of a and d. Note that k in terms of a and d has been already found in Eq. (4) and inserting this equation into Eq. (5) we easily find the following equations for k and Ω:

$$k = m\Lambda^2\left(\frac{\pi^2}{4\left[W\left(\frac{\pi a}{4d}\right)\right]^2}+1\right), \quad \Omega = \frac{\pi\Lambda}{2W\left(\frac{\pi a}{4d}\right)}. \tag{B6}$$

Replacing the above expressions in Eq. (B4) followed by some simple algebra gives

$$Q_1 = \frac{1}{2}ma^2\Lambda^2\left(\frac{\pi^2}{4\left[W\left(\frac{\pi a}{4d}\right)\right]^2}\left\{1-\exp\left[-2W\left(\frac{\pi a}{4d}\right)\right]\right\}+1\right). \tag{B7}$$

APPENDIX C: CALCULATING THE RATIO OF THE ROD'S SWEPT AREA TO THE FILAMENT SWEPT AREA

Under the small-angle approximation, the deflection of a beam, y, with length L as a function of distance with respect to the pivot, x (see Fig. 2), can be easily found by solving the beam equation [29],

$$y(x) = \frac{a}{2L^3}(3Lx^2 - x^3). \tag{C1}$$

By integrating the above equation from 0 to L, the area swept by the filament (curved AD) is

$$S_{AD} = \tfrac{3}{8}aL. \tag{C2}$$

The area swept by the rod (BD) in the case of small deflection is

$$S_{BD} = \tfrac{1}{4}aL. \tag{C3}$$

Dividing Eq. (C3) by Eq. (C2) yields the ratio we seek.

APPENDIX D: CALCULATION OF $\delta\kappa_0$ AND $\delta\kappa$

We know that

$$\kappa_0 = \frac{9\pi\eta^2 L^3}{4\rho R}, \tag{D1}$$

thus for $\delta\kappa_0$ we have

$$\delta\kappa_0 = \kappa_0\left(\frac{\delta\rho}{\rho} + \frac{2\delta\eta}{\eta} + \frac{\delta R}{R} + \frac{3\delta L}{L}\right). \tag{D2}$$

ρ and η can be measured very accurately (as we use the values for the bulk material), a typical value for $\delta R/R$ for a good microsphere is 0.02, and $\delta L/L$ can be considered as 0.01. It means the percentage error for $\delta\kappa_0$ can be almost 5%.

Finding $\delta\kappa$ with the knowledge of $\delta(\kappa/\kappa_0)$ from Eq. (23) and $\delta\kappa_0$ from Eq. (D2) is now straightforward,

$$\delta\kappa = \delta\left(\frac{\kappa}{\kappa_0}\right)\kappa_0 + \frac{\kappa}{\kappa_0}\delta\kappa_0. \tag{D3}$$

[1] E. Unger, K. Boehm, and W. Vater, Electron Microsc. Rev. **3**, 355 (1990).
[2] P. A. Janmey, U. Euteneuer, P. Traub, and M. Schliwa, J. Cell Biol. **113**, 155 (1991).
[3] L. Ma, J. Xu, P. A. Coulombe, and D. Wirtz, J. Biol. Chem. **274**, 19145 (1999).
[4] D. Boal, *Mechanics of the Cell* (Cambridge University Press, Cambridge, 2002).
[5] P. Meurer-Grob, J. Kasparian, and R. H. Wade, Biochemistry **40**, 8000 (2001).
[6] A. Kis, S. Kasas, B. Babic, A. J. Kulik, W. Benoit, G. A. D. Briggs, C. Schonenberger, S. Catsicas, and L. Forro, Phys. Rev. Lett. **89**, 248101 (2002).
[7] J. A. Tuszynski, T. Luchko, S. Portet, and J. M. Dixon, Eur. Phys. J. E **17**, 29 (2005).
[8] S. Portet, J. A. Tuszynski, C. M. Hogue, and J. M. Dixon, Eur. Biophys. J. **34**, 912 (2005).
[9] J. Howard, *Mechanics of Motor Proteins and the Cytoskeleton* (Sinauer, Sunderland, MA, 2001).
[10] O. Lieleg, M. M. A. E. Claessens, C. Heussinger, E. Frey, and A. R. Bausch, Phys. Rev. Lett. **99**, 088102 (2007).
[11] A. Samarbakhsh and J. A. Tuszynski, J. Comput. Theor. Nanosci. **5**, 2041 (2008).
[12] K. M. Taute, F. Pampaloni, E. Frey, and E.-L. Florin, Phys. Rev. Lett. **100**, 028102 (2008).
[13] C. Ni, C. Deck, K. S. Vecchio, and P. R. Bandaru, Appl. Phys. Lett. **92**, 173106 (2008).
[14] K. C. Neuman and S. M. Block, Rev. Sci. Instrum. **75**, 2787 (2004).
[15] K. T. McDonald, Am. J. Phys. **68**, 486 (2000).
[16] J. B. Marion, *Classical Dynamics of Particles and Systems*, 2nd ed. (Academic Press, New York, 1970).
[17] L. A. Segel, *Mathematics Applied to Continuum Mechanics* (Dover, New York, 1987).
[18] R. M. Corless, G. H. Gonnet, D. E. G. Hare, D. J. Jeffrey, and D. E. Knuth, Adv. Comput. Math. **5**, 329 (1996).
[19] W. J. Greenleaf, M. T. Woodside, and S. M. Block, Annu. Rev. Biophys. Biomol. Struct. **36**, 171 (2007).
[20] G. B. Benedek and F. M. H. Villars, *Physics with Illustrative Examples from Medicine and Biology (Statistical Physics)*, 2nd ed. (Springer-Verlag, New York, 2000).
[21] L. Payet (private communication).
[22] M. Kikumoto, M. Kurachi, V. Tosa, and H. Tashiro, Biophys. J. **90**, 1687 (2006).
[23] M. Kurachi, M. Hoshi, and H. Tashiro, Cell Motil. Cytoskeleton **30**, 221 (1995).
[24] P. Venier, A. C. Maggs, M.-F. Carlier, and D. Pantaloni, J. Biol. Chem. **269**, 13353 (1994).
[25] J. C. Kurz and R. C. Williams, Jr., Biochemistry **34**, 13374 (1995).
[26] H. Felgner, R. Frank, and M. Schliwa, J. Cell Sci. **109**, 509 (1996).
[27] H. Felgner, R. Frank, J. Biernat, E.-M. Mandelkow, E. Mandelkow, B. Ludin, A. Matus, and M. Schliwa, J. Cell Biol. **138**, 1067 (1997).
[28] F. Gittes, B. Mickey, J. Nettleton, and J. Howard, J. Cell Biol. **120**, 923 (1993).
[29] J. M. Gere and S. P. Timoshenko, *Mechanics of Materials*, 3rd ed. (Chapman and Hall, London, 1991).